EPSC Abstracts
Vol. 5, EPSC2010-759, 2010
European Planetary Science Congress 2010

Principal component spectral matching of laboratory and MESSENGER observations and compositional units on Mercury

Mario D'Amore (1), Jörn Helbert (1), Alessandro Maturilli (1), Noam R. Izenberg (2), Ann L. Sprague (3), Gregory M. Holsclaw (4), James W. Head (5), William E. McClintock (4), Deborah L. Domingue (6) and Sean C. Solomon (7).

(1) DLR, Berlin, Germany (Mario.DAmore@dlr.de).
(2) Johns Hopkins University Applied Physics Laboratory, Laurel, MD 20723, USA.
(3) Lunar and Planetary Laboratory, University of Arizona, Tucson, AZ 85721, USA.
(4) Laboratory for Atmospheric and Space Physics, University of Colorado, Boulder, CO 80303, USA.
(5) Department of Geological Sciences, Brown University, Providence, RI 02912, USA.
(6) Planetary Science Institute, 1700 E. Fort Lowell, Suite 106 Tucson, AZ 85719.
(7) Department of Terrestrial Magnetism, Carnegie Institution of Washington, Washington, DC 20015, USA.

Abstract

We have analyzed reflectance spectra of Mercury's surface obtained by the Mercury Atmospheric and Surface Composition Spectrometer instrument on MESSENGER during the spacecraft's first two flybys of Mercury to characterize and distinguish surface compositional units. We applied a statistical technique to extract the underlying relationships among units. Without applying photometric corrections, we were able cluster surface observations into different classes that correspond to geomorphological units identified from MESSENGER images, such as the smooth plains in Rudaki crater and the heavily cratered neighboring terrain. We then applied biconical reflectance spectra from the DLR Planetary Emissivity Laboratory to assess possible major constituents of Mercury surface materials.

1. Introduction

During the first two MESSENGER flybys of Mercury, the Mercury Atmospheric and Surface Composition Spectrometer (MASCS) [1, 2] obtained reflectance spectra of large areas of the planet's surface. The resulting dataset is composed of several hundred spectra that have not yet been corrected for effects of observing geometry or photometry. Under the hypothesis that surface compositional information can be efficiently separated from other contributions by the use of statistical techniques, we have employed principal component and clustering analyses to identify and characterize spectral units along the MASCS ground tracks.

2. Data Analysis

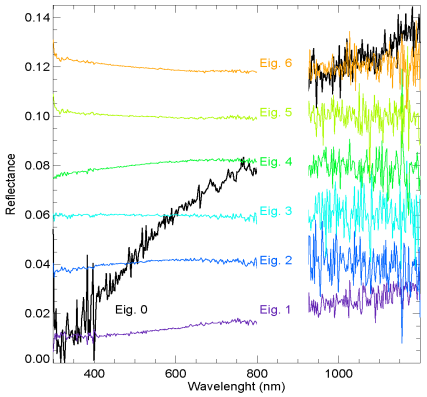

Fig 1. Eigenvectors extracted for the entire spectral range, each shifted by 0.01 in reflectance for clarity.

To retrieve and characterize the number and spectral shapes of the different components present in the dataset, we apply principal component analysis (PCA), a well-established technique in remote sensing [3–5]. PCA expresses the data in a new vectorial basis set, for which the data covariance is minimized. PCA essentially reduces the dimensionality of the dataset and allows modeling of the data as a linear combination of the principal components or eigenvectors. The dimensionality of

the new basis set measures the number of components that influence the system.

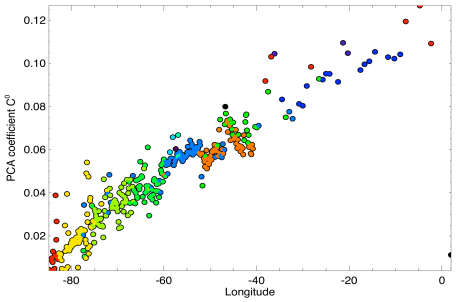

Fig. 2. Concentration coefficients extracted from the C matrix corresponding to the first eigenvector in Fig. 1. Color codes are relative to the distinct clusters found with a hierarchical clustering algorithm (see text and Fig. 4).

Finding the crossing point between principal and secondary eigenvalues is thus a primary task of PCA. In particular, we evaluated the eigenvalue ratio [3] and the reconstruction error, and we inspected visually the goodness of fit of spectra to the model. Applying the covariance matrix decomposition, spectra in the dataset are assembled in matrix form as

$$\mathbf{D} = \mathbf{R}\,\mathbf{C} \qquad (1)$$

where **D** is the matrix of the data, **R** the matrix of reconstruction vectors, and **C** the matrix of relative concentration coefficients. The goal of PCA is to decompose **D** into two matrices. **R** will consist of the principal eigenvectors calculated from the covariance matrix of **D,** $\mathbf{S_D}$. There is no unique solution to this problem, and it is a common situation in remote sensing to have more equations than unknowns, resulting in an overdetermined system. An estimation of the vectors needed to reconstruct the data given the noise is the essential step toward solving the problem and converging on an accurate solution. Because of the wide spectral range of the data, we choose to apply the analysis to the entire range and separately also to the visible (VIS) and the near-infrared (NIR) channels, in order to monitor potential differences in behavior between those portions of the spectrum. Application to the full MASCS dataset shows that in general seven eigenvectors are sufficient to reconstruct the data within the error. The eigenvectors obtained from an analysis only of the VIS observations do not differ strongly from those obtained with the full dataset. The extracted eigenvectors for the entire spectral range are shown in Fig. 1. A comparison of the two channels indicates that the NIR portion is carrying significantly less information than the VIS portion. Each spectral eigenvector can be regarded as a representative of a distinct spectral class that varies in abundance along the track. The first eigenvector always displays a strong positive or "red" slope, probably strongly linked to effects associated with viewing geometry variations, and all eigenvectors show distinctive spectral signatures.

The concentration coefficients in the **C** matrix indicate that spectral units show substantial geographical variation.

Because we do not photometrically correct the data, we can clearly see the dependence of the coefficients on geometrical parameters (namely, emission angle in Fig. 3). We apply a decorrelation technique to partially remove dependence on observation angle in the retrieved concentration coefficients. We construct the matrix $\mathbf{C'}$ as $\{\mathbf{c_1},\ldots,\mathbf{c_n},\mathbf{e}\}$, where $\mathbf{c_i}$ are rows of **C** and **e** is a vector of the emission angles. $\mathbf{S_{C'}}$ is then the covariance matrix of $\mathbf{C'}$ and can be calculated from

$$\mathbf{S_{C'}} = \mathbf{n^{-1}}\,\mathbf{C'^{T}}\,\mathbf{H}\,\mathbf{C'} \qquad (2)$$

where $^{\mathbf{T}}$ denotes the transposition operator, *n* is the number of columns of **C,** and **H** is the centering matrix, defined as

$$\mathbf{H} = \mathbf{I} - n^{-1}\mathbf{J} \qquad (3)$$

where **I** is the identity matrix and **J** is a matrix where all elements equal 1. Finally, the transformed matrix **Z** is defined by

$$\mathbf{Z} = \mathbf{H}\,\mathbf{C'}\mathbf{S_{C'}}^{-1/2} \qquad (4)$$

and is also called the Mahalanobis transform of matrix **C**. It has the peculiar property that its covariance matrix is the identity matrix

$$\mathbf{S_Z} = \mathbf{I} \qquad (5)$$

or, in other words, the rows and columns of Z are decorrelated [9]. Now we can extract the first *n* rows of **Z** that correspond to the eigenvectors of the

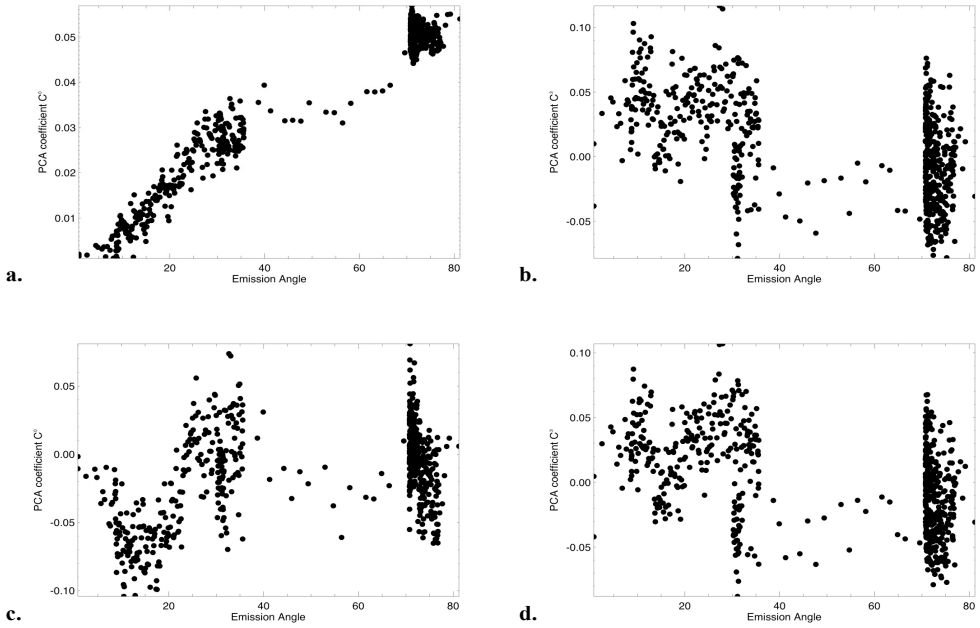

Fig. 3. Concentration coefficients from matrix **C** versus the emission angle. **(a)** and **(b)** correspond to the first and the fourth eigenvectors, respectively. **(c)** and **(d)** are the corresponding rows from the **Z** matrix, that is, the transformed **C′** matrix. The strong dependency of the first coefficient on the emission angle is greatly reduced after the transformation, whereas the fourth coefficient remains almost unchanged.

concentration coefficients in **C′**. Now we can extract the first n rows of **Z** that correspond to the eigenvectors of the concentration coefficients in **C′** and in **C**. We thus obtain the decorrelated concentration coefficients (or **C** via the Mahalanobis transformation). This set does not satisfy the relation (1) and therefore cannot linearly reconstruct the original dataset. The decorrelation removes the main variation directly linked to variations in illumination and viewing geometry. Nevertheless, it retains a variation (Fig. 4) along track that we suppose is the result of actual variation in reflectance across the surface. In particular, the locations of spectrally distinct units correlate well with those inferred from color imaging (Fig. 4). The DLR Planetary Emissivity Laboratory (PEL) is in the final testing phase for a new setup that will allow measurement of emissivity at Mercury temperatures and wavelengths near 1 mm [6]. In the meantime we make use of newly available visible–near-infrared (VNIR) biconical reflectance spectra from PEL [7] to assist in the identification of the possible constituents of each spectral unit. We employ a target transformation (TT) to seek linear combinations of the eigenvectors estimated by PCA that yield a set of laboratory-derived spectral components that can closely reproduce the original spectra [8]. In practice, this step is achieved by projecting a laboratory test spectrum onto the space spanned by the eigenvectors [3]. If the test spectrum fits within the dimensionality of the data, it is a component of the system and a possible spectral end-member and will be closely reconstructed using a combination of the derived eigenvectors. If not, it will be poorly reconstructed by the eigenvectors. In this way, the target

transformation presents a tool for identifying spectral end-member components within a system.

Laboratory conditions are designed to mimic observational parameters for spectra obtained at Mercury. Moreover, mineral selection is based on expectations for Mercury's surface, as well as high-temperature changes in behavior documented at PEL for some materials.

6. Summary and Conclusions

We observed the presence of isolated spectral units on Mercury that show a strong correlation with surface units mapped by the MESSENGER imaging system. At the same time, we have begun to make use of the newly available VNIR biconical reflectance observations from our Planetary Emissivity Laboratory as a basis for testing possible surface constituents. We use these data as a temporary substitute for upcoming high-temperature measurements that will allow us to achieve more precise results.

References

[1] McClintock, W.E., et al., Science, 321, 92-94, 2008.

[2] Izenberg, N.R., et al., Eos Trans. AGU, 89(53), Fall Meet. Suppl., abstract U11C-05, 2008.

[3] Bandfield, J.L., et al., J. Geophys. Res., 105, 9573-9588, 2000.

[4] Ramsey, M.S., Christensen P.R., J. Geophys. Res., 103, 577-596, 1998.

[5] Smith, M.D., et al., J. Geophys. Res., 105, 9539-9552, 2000.

[6] Helbert, J., et al., EPSC 2010, this conference, 2010.

[7] Maturilli, A., et al., EPSC 2010, this conference, 2010.

[8] Malinowski, E.R., *Factor Analysis in Chemistry*, John Wiley, New York, 1991.

[9] Salomon, D., Data Compression: The Complete Reference, Springer, Berlin, 1092 pp., 2006.

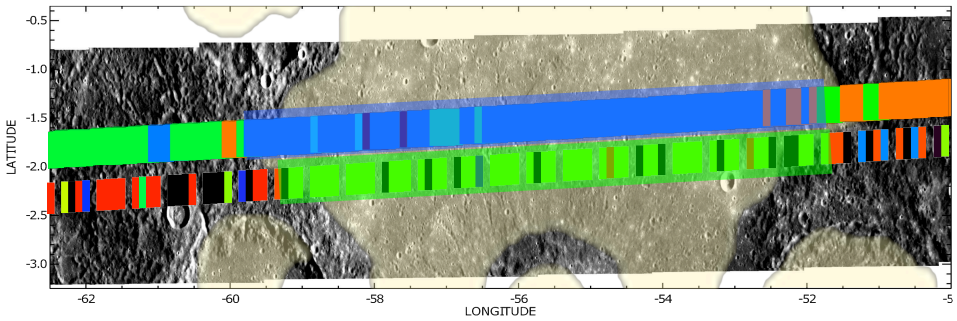

Fig 4. Units found feeding the clustering algorithm with the subset of the **Z** matrix. The upper strip was calculated from MASCS spectra and uses the same color code as in Fig. 2. The bottom strip, shifted for clarity, was calculated by extracting the average MDIS reflectance value over pixels that fell on the MASCS footprints. The MDIS color code is related to clusters found from separate clustering analysis. We note how the blue clusters from the upper strip and the green cluster from the bottom strip are concentrated mainly within the Rudaki crater.